ELSEVIER

Automation in Construction 13 (2004) 21–35

AUTOMATION IN CONSTRUCTION

www.elsevier.com/locate/autcon

Reconstructing images of barcodes for construction site object recognition☆

David E. Gilsinn[a,*], Geraldine S. Cheok[b], Dianne P. O'Leary[c]

[a] National Institute of Standards and Technology (NIST), Information Technology Laboratory, Mathematical and Computational Sciences Division, Gaithersburg, MD 20899-8910, USA

[b] NIST, Building and Fire Research Laboratory, Construction Metrology and Automation Group, Gaithersburg, MD 20899-8611, USA

[c] Computer Science Department, University of Maryland, College Park, MD 20742, USA

Abstract

This work investigates the potential for using LADAR to read barcodes at a range of 10–40 m. The first step is to choose appropriate materials for the barcode and collect data for both the images of bars at various distances and the characteristics of the LADAR beam. The second step is to develop a mathematical model for how intensity images are distorted by LADAR optics and to study how the images might be reconstructed. Our model is a linear convolution equation, and we solve for the original image through a regularized least squares problem. We present the results of our experiments along with evidence that the proprietary LADAR data processing introduces considerable nonlinearities, which must be understood in order to achieve good reconstructions.

Keywords: Barcodes; Deconvolution; Image processing; LADAR; Object recognition; Sparse matrix

1. Introduction

Imaging sensors such as LADARs (laser distance and ranging devices) are used to rapidly acquire data of a scene to generate three-dimensional (3D) models. They are used to obtain two- or three-dimensional arrays of values such as range, intensity or other characteristics of a scene. Currently available LADARs can gather four pieces of information-range to an object, two spatial angular measurements and the strength of the returned signal (intensity). Various methods are used to convert the data, which are collected in the form of point clouds, into meaningful 3-D models of the actual environment for visualization and scene interpretation. The points within a point cloud are indistinguishable from each other with regard to their origin; i.e., there is no way to tell if a point is reflected from a tree or from a building. As a result, the methods used to generate surface models treat all points identically and the results are indistinguishable "humps/bumps" in the scene surface. Current surface generation methods, using LADAR data, require intensive manual intervention to recognize, replace and/or remove objects within a scene. As a result, aids to object identification have been recog-

☆ Official contribution of the National Institute of Standards and Technology; not subject to copyright in the United States.

* Corresponding author.

E-mail addresses: dgilsinn@nist.gov (D.E. Gilsinn), cheok@nist.gov (G.S. Cheok), oleary@nist.gov (D.P. O'Leary).

0926-5805/$ - see front matter © 2003 Published by Elsevier B.V.
doi:10.1016/j.autcon.2003.08.003

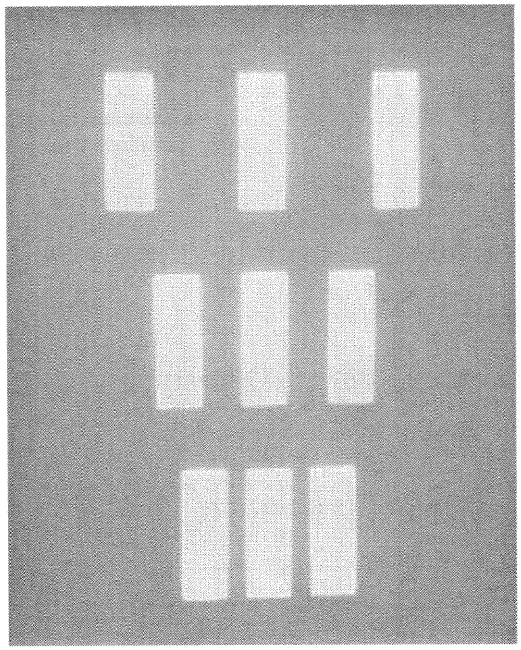

Fig. 1. Photograph of one set of the bar codes.

nized by the end users as a highly desirable feature and a high priority area of research.

The use of barcodes or Universal Product Code (UPC) symbols has become the universal method for the rapid identification of objects ranging from produce to airplane parts. The same method could also be used to identify objects within a construction scene. This would involve using the LADAR to "read" a barcode. The concept is to use the intensity data from the LADAR to distinguish the bar pattern. The advantage of this concept is that no additional hardware or other sensor data is required to gather the additional data. The basis for this concept lies in the high intensity values obtained from highly reflective materials.

The challenges are the ability to read the barcode from 100 m or greater, distinguish barcode points from the other points in the scene, capture a sufficient number of points to define the barcode for correct identification, and the ability to read barcodes that are skewed.

At ISARC 2001 [1], methods of determining the appropriate material for the barcodes and determining if the use of barcodes was viable were reported. The results from these efforts showed that, at distances beyond 20 m (Figs. 1 and 2), the intensity images were too blurred to be readable and that image processing techniques were necessary to reconstruct the image. The blurring or convolution of the image is a result of the low resolution (number of pixels/unit area; a consequence of the instrument's angular resolution) of the intensity images at larger distances and of distortion of the intensity image by the LADAR optics. As a result, an investigation of possible methods to de-blur (deconvolve) the intensity images was conducted. Deconvolution of the image involves re-

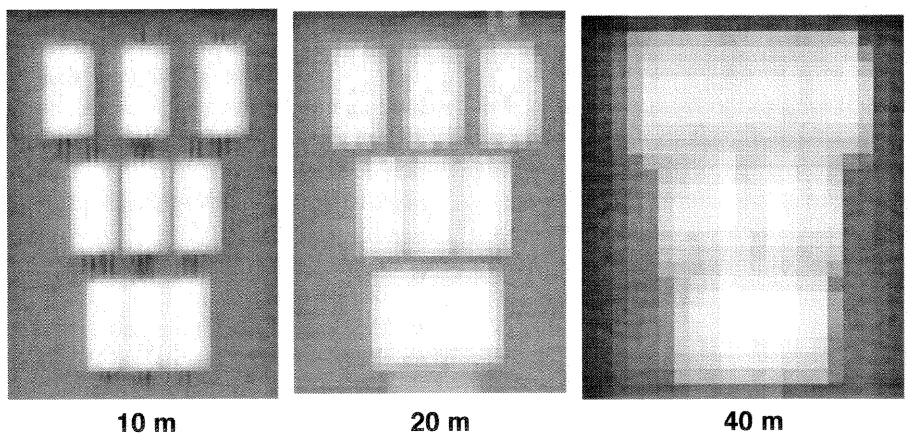

Fig. 2. LADAR images of the bar codes at three distances. Note the distorting of the image with distance.

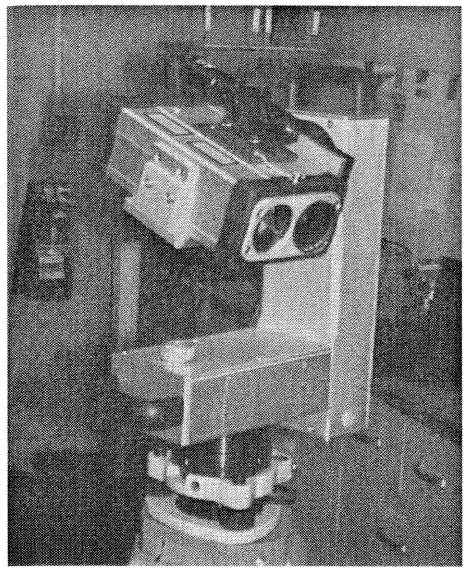

Fig. 3. LADAR scanner.

versing the convolution, implying that, if the convolution process was known, the image may be reconstructed. The results of the deconvolution study are reported here. This paper represents a case study of the extent to which classic image processing techniques can be directly applied to reconstructing LADAR intensity images.

The paper is divided as follows. Section 2 briefly describes the experimental acquisition of the barcode data. Section 3 discusses some problems associated with the acquired data. Section 4 describes physical measurements of the LADAR beam. Section 5 introduces an optics distortion model. Section 6 discusses an algorithm for image reconstruction. Section 7 describes the numerical results related to barcode reconstruction. Finally, Section 8 presents some discussion and conclusions.

2. Experimental considerations

The LADAR, shown in Fig. 3, selected for the experiment, uses a pulsed laser and is mounted on a pan-tilt device whose horizontal and vertical movements are controlled by two stepper motors. It returns four pieces of information-range, two spatial angular measurements and intensity. The intensity is a dimensionless quantity that ranges from 0 to 255 (most reflective), which is based on the strength of the return signal. In order to "read" the barcode, its existence has to be first established. To establish its existence, the barcode has to have a unique feature or characteristic so that it is easily identifiable. Therefore, the barcode would have to be made of a material that makes it easily distinguishable from any

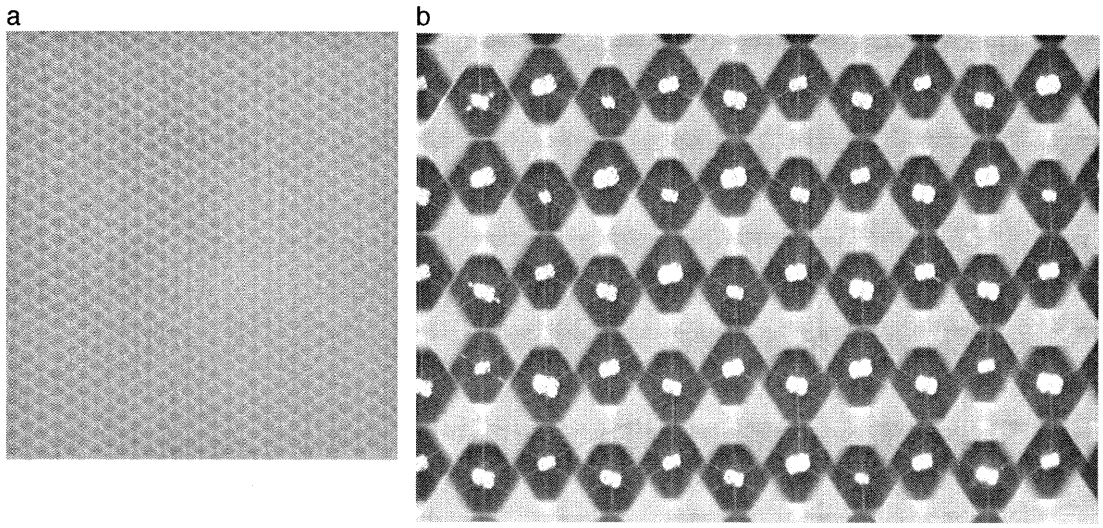

Fig. 4. (a) Photograph of the reflective material. (b) Magnified photo. Width represents 1.5 mm of surface.

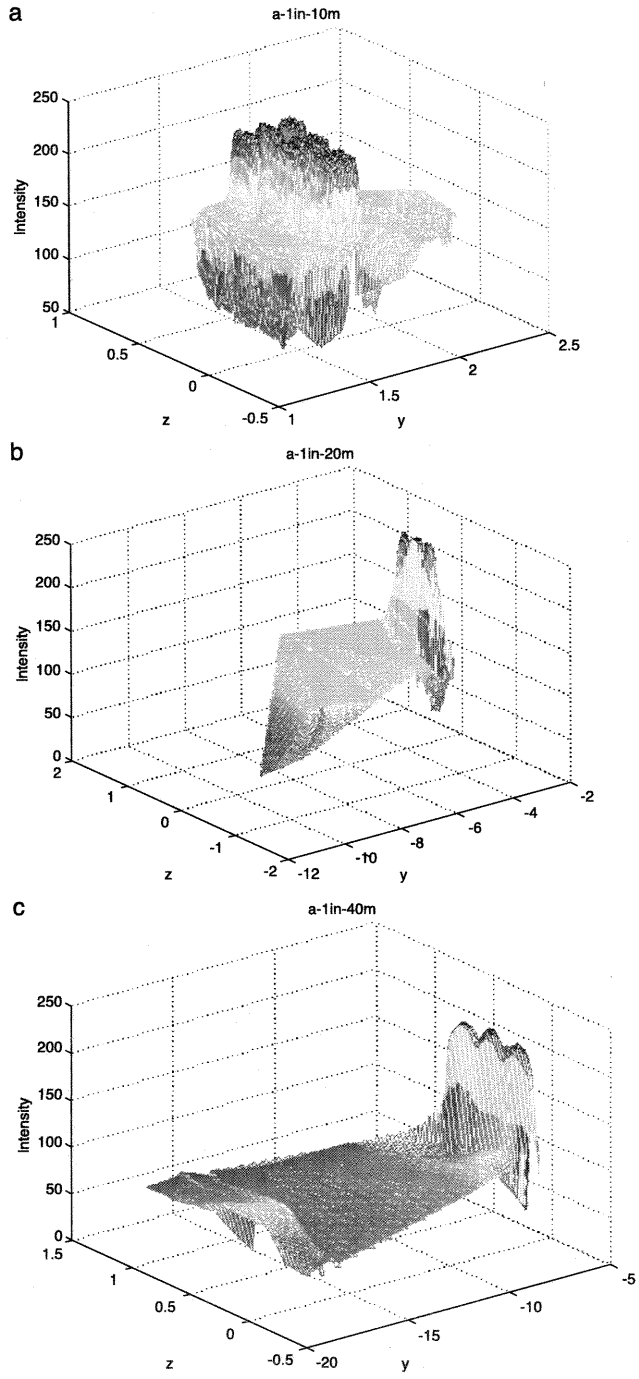

Fig. 5. (a) Raw intensity data of 25.4 mm (1 in.) bars at 10 m. (b) Raw intensity data of 25.4 mm (1 in.) bars at 20 m. (c) Raw intensity data of 25.4 mm (1 in.) bars at 40 m.

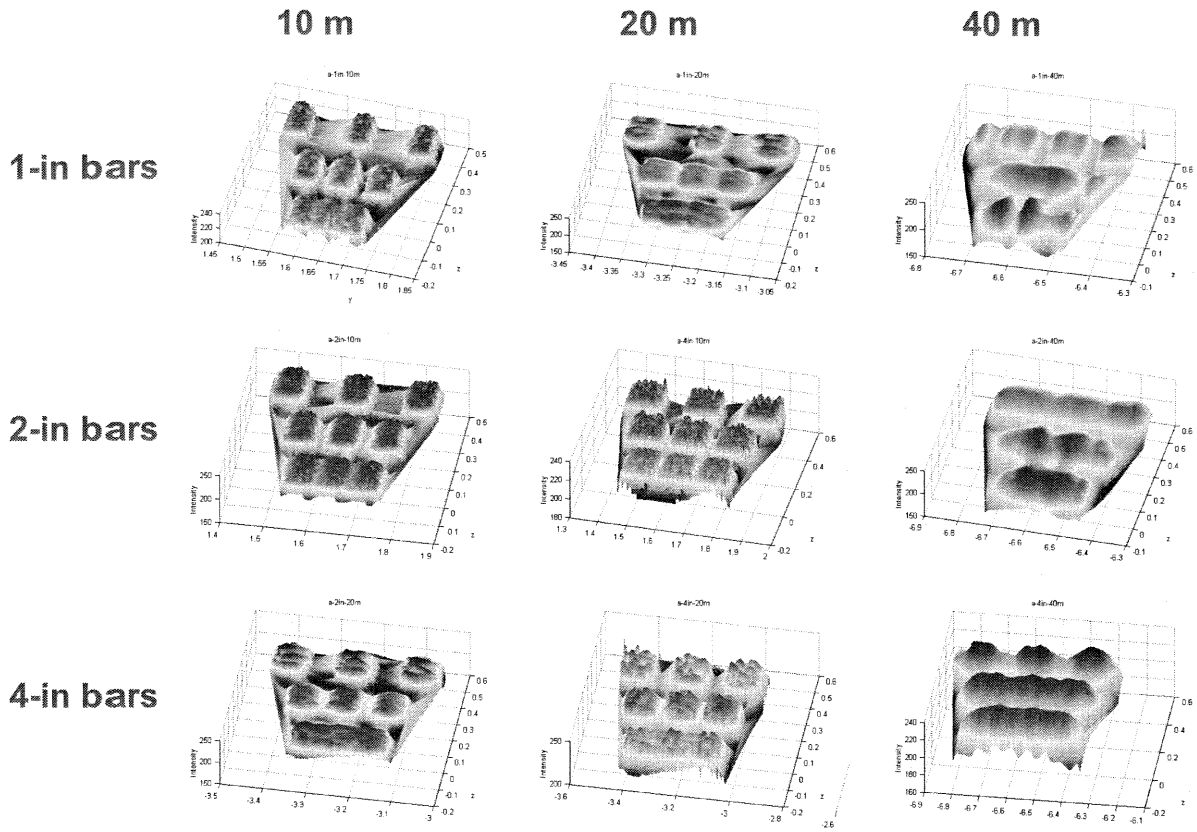

Fig. 6. Pre-processed LADAR images of the nine data sets examined.

background material based on the returned intensity value. A good candidate material would be one that that would return an intensity that was both much higher than any other material commonly found at a construction site and that was consistently high for distances of 0–150 m, i.e., intensity did not drop off with distance. A reflective sheeting, that is a highly reflective prismatic lens sheeting used for traffic signage, was used to construct the barcodes of Fig. 1. This material was chosen as it was readily available, durable and would reflect light even if skewed away from the light source. Sample photographs of the sheeting material are shown in Fig. 4. Fig. 4b shows that the sheeting is made of an array of prisms, each of which has the capability of reflecting light in the direction from which it entered the prism.

3. LADAR image considerations

In this section, we wish to discuss two items related to the data acquired from the LADAR. The first relates to the fact that a LADAR can only be approximately oriented towards a desired object and that the ensuing scan picks up peripheral background data. The images therefore must be pre-processed to eliminate the undesirable data. The second item involves the scan results obtained from the LADAR used for this study. In particular, the scanned data seems to indicate that the entire process of acquiring the data by the LADAR produces a horizontal broadening of the ground truth image but no significant vertical broadening. This suggests that the process is non-linear and that traditional linear image processing algorithms could only produce limited results.

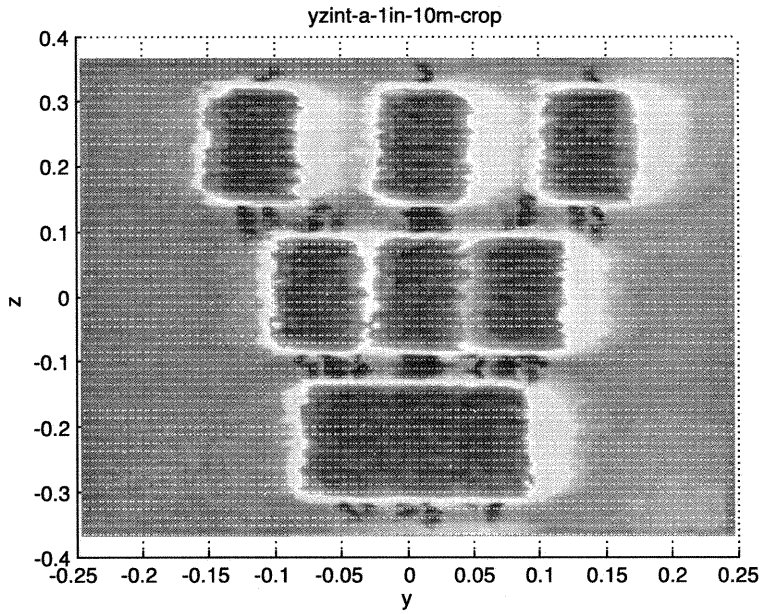

Fig. 7. Vertical view of the scanned data of 25.4 mm (1 in.) bars at 10 m.

Regarding the first item, the presence of barcodes can be established by examining the plots of the intensity values vs. the location as seen in Fig. 5. The elevated portions of the surface (mountains) are where the barcodes are located. The background data is shown as waterfall data along the edges of Fig. 5a as well as the extended "sheets" of data in all of the figures. In order to isolate the barcodes, the data had to be pre-processed using an intensity histogram technique described previously in ISARC 2001 [1]. The resulting pre-processed images, with the background points removed, are shown in Fig. 6.

An examination of the data in Fig. 6 shows a clear broadening of the intensities in the horizontal direction. In order to estimate the order of magnitude of the broadening, the subfigures in Fig. 6 were displayed so that one could look vertically downward and measure the horizontal and vertical scales of the highest intensity data. An example of this display is given in Fig. 7. This figure shows the *Y*-axis and *Z*-axis scales in meters (*X*-axis is always assumed to be perpendicular to the target). The units for the original barcodes are 152.4×25.4 mm (6×1 in.). However, the approximate units for the scanned image are 152.4×50.8 mm (6×2 in.). This translates to an approximate 100% increase in the horizontal spread and a 0% increase in the vertical spread.

4. Beam size and divergence estimation

In order to develop a model for image reconstruction, it was necessary to understand the divergence of the laser beam, i.e., how the laser beam changed as a function of distance. The data for determining the beam size was obtained by measuring the dimensions

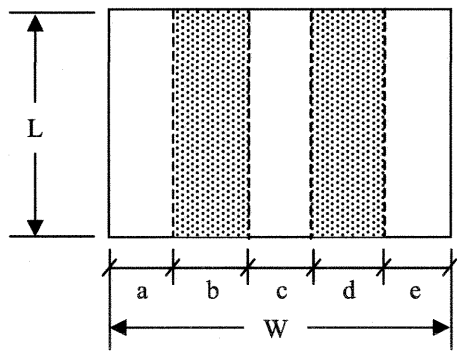

Fig. 8. "a", "c" and "e" are the widths of the bright bands, and "b" and "d" are the widths of the dark bands.

Table 1
Average height and widths in millimeters of the bright and dark bands of the beam shown in Fig. 8

	10 m	20 m	40 m
L	27.5	56.2	108
W	52.4	64	111
a	–	12.7	15
b	–	13.2	25
c	–	14.7	22.3
d	–	11.7	30.5
e	–	12	18

of the laser beam outline as projected on a white target. An infrared viewer was necessary to see the projection of the laser on the target so that an outline of the beam could be drawn. The outline of the beam was drawn by two or more observers, and the measurements were averaged. The LADAR uses a laser, which consists of three laser diodes. The projection of the laser beam on the target was seen as a bright rectangle for distances less than 10 m and three bright vertical bands separated by dark bands for distances greater than 10 m. A schematic of the beam is shown in Fig. 8. A subset of the measurements of the beam size at various distances is given in Table 1.

The average vertical beam divergence was 2.14 mrad ($\sigma = 0.39$ mrad) and the average horizontal beam divergence, excluding an outlier (negative divergence) was 1.86 mrad ($\sigma = 0.44$ mrad). The average beam divergence (horizontal and vertical combined) was 2.01 mrad ($\sigma = 0.43$ mrad)—compared with the manufacturer's specified divergence of 3 mrad. The lower experimental value was likely a result of the inability of the unaided human eye to detect the faint edges of the laser beam projection. A schematic of the diverging beam is shown in Fig. 9.

5. Optics model for beam distortion

For the purpose of developing an optics model of the distortion process involved with LADAR imaging, we assume that there exists a data set representing barcodes on a 1×1-m board with intensity levels ranging from 0 to 255. This data set will be called the *ground truth*. We will discretize the ground truth image by defining: $0 = y_1 < y_2 < \ldots < y_{nf} = 1$, $0 = z_1 < z_2 < \ldots < z_{nf} = 1$, $\Delta y_i = y_{i+1} - y_i = \Delta z_j = z_{j+1} - z_j = \Delta$. The intensity at patch $\Delta y_i \Delta z_j$ is given by $f(y_i^*, z_j^*)\,\Delta y_i \Delta z_j$ where f is a function of (y, z) expressing the intensity response at some point (y_i^*, z_j^*) in the patch. Due to distortions, the LADAR image of the response from the barcode surface is smeared into some form of blurred spot shown in Fig. 10. For simulation purposes, the distorted image will be taken as a subset (to be defined below) of the ground truth image. Points in the distorted image will be identified by (Y, Z) and those in the ground truth image by (y, z). These are different notations for points in the same axis system.

The distortion at a point (Y, Z) due to a point (y, z) can be described by a function $h(y, z; Y, Z)$, called the *beam spread function*. For most practical purposes, the beam spread function can be considered translation invariant in the sense that its distortion value only depends on the distance between (Y, Z) and (y, z) so that h has the form $h(Y - y, Z - z)$ (see Fig. 11). The incremental distortion effect at (Y, Z) due to a neighboring patch of (y, z) is $g(Y, Z) = h(Y - y, Z - z) f(y, z)\,\Delta y \Delta z$. To describe the total effect $g(Y, Z)$ of all of the points (y, z) in the ground truth image, one sums over all of the patches in the ground truth image. As the number of grid points nf in the ground truth image grows and the patch size tends to 0, the sum can be replaced by an integral. This integral is called a *convolution integral*.

$$g(Y,Z) = \int_{-\infty}^{\infty}\int_{-\infty}^{\infty} h(Y-y, Z-z) f(y,z)\,\mathrm{d}y\mathrm{d}z \qquad (1)$$

Assume that the distorted image g is sampled at ng points $(Y_p = (p-1)\Delta, Z_q = (q-1)\Delta)$ for $p, q = 1, \ldots, ng$,

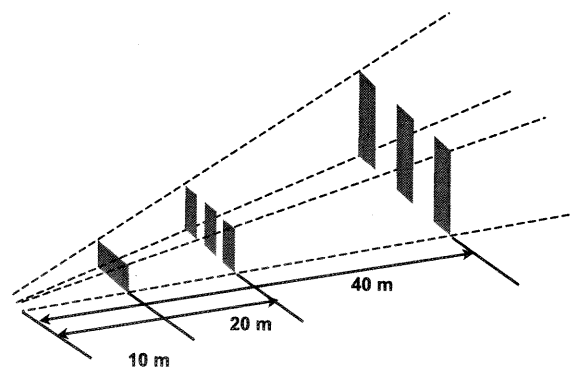

Fig. 9. Diverging beam schematic.

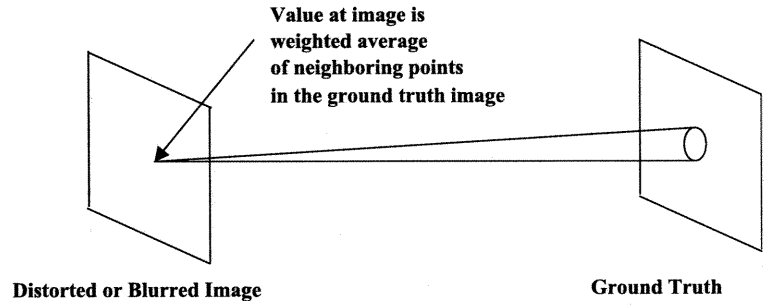

Fig. 10. Distortion on the image caused by averaging of pixels in the ground truth image.

forming a vector $\boldsymbol{G}$ of ng^2 elements. Let the model, h, of the beam spread function be sampled at $(ma)^2$ points $(i\Delta, j\Delta)$, for $i, j = -k, -k+1, \ldots, k-1, k$. This gives a total of ma^2 data values $\widehat{H}$, where $ma = 2k+1$, and we define all other values of our approximation of h to be zero. Assume that we approximate the ground truth image by $f((i-1)\Delta, (j-1)\Delta) \approx F(i, j)$ for $i, j = 1, \ldots, nf$, and again arrange these values as a vector. Then, our convolution integral can be approximated by

$$G(p,q) \approx \sum_{i=1}^{nf} \sum_{j=1}^{nf} \widehat{H}(p-i, q-j) F(i,j) \Delta y_i \Delta z_j \qquad (2)$$

This gives ng^2 linear conditions on nf^2 unknowns $F(i, j)$. Let $\mathbf{H}$ be the matrix derived from the values $\widehat{H}$ so that our approximation becomes $\boldsymbol{G} \approx \mathbf{HF}$. These relations are illustrated in Fig. 11.

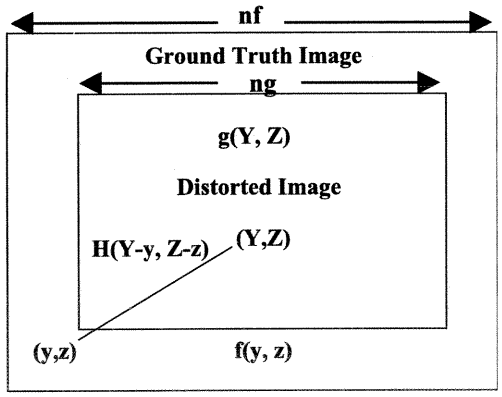

Fig. 11. Distorted image overlaid on the ground truth image.

6. Computational aspects for image restoration

Since the ground truth image $\mathbf{F}$ is larger than the distorted image $\boldsymbol{G}$, there are more degrees-of-freedom involved in reconstructing $\mathbf{F}$ from a measured $\boldsymbol{G}$. A computable approach is to determine $\mathbf{F}$ in a least squares manner to satisfy

$$\min_F \| \mathbf{HF} - \mathbf{G} \|^2. \qquad (3)$$

This is an ill-posed problem since there may not be a single solution. In fact, it is known that if $\mathbf{F}$ is combined with high frequency sinusoidal data, then, under convolution, it produces the same $\boldsymbol{G}$. A penalty term can be added to this minimization problem that puts a premium on the size of $\mathbf{F}$ selected. Introduce $\lambda > 0$ and form the following minimization problem

$$\min_F \left\{ \| \mathbf{HF} - \mathbf{G} \|^2 + \lambda \| \mathbf{F} \|^2 \right\} \qquad (4)$$

The second term is called a regularization term and its function is to control the magnitude of the final $\mathbf{F}$. In practice, λ is selected as a small positive number. In our case, we used a λ of 0.001.

We solve the least squares problem using the LSQR algorithm of Paige and Saunders [2]. This algorithm never modifies elements of $\mathbf{H}$ and uses the matrix only to form products $\mathbf{H}\boldsymbol{y}$ with various vectors $\boldsymbol{y}$. Thus, we need only store the ma^2 coefficients of $\widehat{H}$ rather than the $ng^2 \times nf^2$ matrix $\mathbf{H}$. It is an iterative algorithm since the matrix $\mathbf{H}$ is large and sparse. It should also be noted that, by a reorganization of the computation, it is possible to reverse the roles played by $\mathbf{H}$ and $\mathbf{F}$ and use the same algorithm to

estimate a beam spread function given knowledge of the ground truth image and the scanned image. A brief discussion of the results of some sample calculations will be given below.

The essence of the algorithm is that problem (4) is reduced to a smaller least squares problem (see Eq. (15) below) that can be solved inexpensively. This permits solving large problems by minimizing memory storage requirements. One begins the algorithm by using a fundamental result from Golub and Kahan [3]. Any real $m \times n$ matrix $\mathbf{H}$ can be decomposed as

$$\mathbf{H} = \mathbf{U}\mathbf{B}\mathbf{V}^T \tag{5}$$

where $\mathbf{U}$ and $\mathbf{V}$ are orthogonal matrices. That is, $\mathbf{U}^T\mathbf{U} = \mathbf{U}\mathbf{U}^T = \mathbf{I}$, $\mathbf{V}^T\mathbf{V} = \mathbf{V}\mathbf{V}^T = \mathbf{I}$. $\mathbf{B}$ is a bidiagonal matrix of the form

$$\mathbf{B} = \begin{bmatrix} \alpha_1 & 0 & \cdots & 0 \\ \beta_2 & \alpha_2 & \cdots & 0 \\ \vdots & \ddots & \ddots & \vdots \\ 0 & \cdots & \beta_n & \alpha_n \end{bmatrix} \tag{6}$$

A similar result is true if $\mathbf{H}$ has complex entries. Now, using the orthogonality property of $\mathbf{U}$ and $\mathbf{V}$, it is clear that

$$\mathbf{H}\mathbf{V} = \mathbf{U}\mathbf{B}$$

$$\mathbf{H}^T\mathbf{U} = \mathbf{V}\mathbf{B}^T \tag{7}$$

If orthogonal matrices $\mathbf{U}$ and $\mathbf{V}$ are found that satisfy the above conditions, then this least squares problem can be reduced to a simpler form. By orthogonality, we always have $\|z\| = \|\mathbf{U}^T z\|$ so that

$$\begin{aligned} \|\mathbf{H}\mathbf{F} - \mathbf{G}\| &= \|\mathbf{U}\mathbf{B}\mathbf{V}^T\mathbf{F} - \mathbf{G}\| \\ &= \|\mathbf{U}^T(\mathbf{U}\mathbf{B}\mathbf{V}^T\mathbf{F} - \mathbf{G})\| \\ &= \|\mathbf{B}\mathbf{V}^T\mathbf{F} - \mathbf{U}^T\mathbf{G}\| \end{aligned} \tag{8}$$

Let $\mathbf{U}$ be given columnwise by

$$\mathbf{U} = [u_1, u_2, \cdots, u_n]^T \tag{9}$$

where

$$u_1 = \frac{\mathbf{G}}{\|\mathbf{G}\|} \tag{10}$$

Then, since $\mathbf{U}$ is orthogonal,

$$\mathbf{U}^T\mathbf{G} = \begin{bmatrix} u_1^T\mathbf{G} \\ u_2^T\mathbf{G} \\ \vdots \\ u_n^T\mathbf{G} \end{bmatrix} = \begin{bmatrix} \beta_1 \\ 0 \\ \vdots \\ 0 \end{bmatrix} = \beta_1 \begin{bmatrix} 1 \\ 0 \\ \vdots \\ 0 \end{bmatrix} = \beta_1 e_1 \tag{11}$$

For notation, e_k is the vector of all zeroes with one in the kth element and $\beta_1 = \|\boldsymbol{G}\|$. With this notation, one has

$$\|\mathbf{H}\mathbf{F} - \mathbf{G}\| = \|By - \beta_1 e_1\| \tag{12}$$

where $\boldsymbol{y} = \mathbf{V}^T\mathbf{F}$. Thus, the previous least squares problem can be reduced to the new minimization problem

$$\min_y \|By - \beta_1 e_1\| \tag{13}$$

A regularization term can be introduced by solving the minimization problem

$$\min_y \left\| \begin{bmatrix} B \\ \lambda I \end{bmatrix} y - \begin{bmatrix} \beta_1 e_1 \\ 0 \end{bmatrix} \right\| \tag{14}$$

The algorithm of Paige and Saunders [2] proceeds iteratively so that, after $k+1$ steps of the Golub and Kahan [3] bidiagonalization process, one has

$$\beta_1 = \|\mathbf{G}\|$$

$$U_{k+1} = [u_1,\ u_2,\ \cdots,\ u_{k+1}]$$

$$V_{k+1} = [v_1,\ v_2,\ \cdots,\ v_{k+1}]$$

$$B_k = \begin{bmatrix} \alpha_1 & & & & & \\ \beta_2 & \alpha_2 & & & & \\ & \beta_3 & \alpha_3 & & & \\ & & \ddots & \ddots & & \\ & & & \ddots & \ddots & \\ & & & & \ddots & \alpha_k \\ & & & & & \beta_{k+1} \end{bmatrix} \tag{15}$$

The kth approximation to the solution F is defined by $F_k = V_k y_k$ where y_k solves the kth iteration problem

$$\min_{y_k} \left\| \begin{bmatrix} B_k \\ \lambda I \end{bmatrix} y_k - \begin{bmatrix} \beta_1 e_1 \\ 0 \end{bmatrix} \right\| \tag{16}$$

If we define the following residuals

$$t_{k+1} = \beta_1 e - B_k y_k$$

$$r_k = \mathbf{G} - \mathbf{H}F_k \tag{17}$$

then Paige and Saunders [2] show that the relations

$$r_k = U_{k+1} t_{k+1} \tag{18a}$$

$$\mathbf{H}^T r_k = \lambda^2 F_k + \alpha_{k+1}\tau_{k+1} v_{k+1} \tag{18b}$$

hold to the accuracy of the computer. In Eq. (18b), τ_{k+1} represents the last component of $t_{k+1}=[\tau_1,\ \tau_2,\ \ldots,\ \tau_{k+1}]$. Eq. (19) also shows that F_k, with residual r_k, is an acceptable solution of

$$\min_x \left\| \begin{bmatrix} \mathbf{H} \\ \lambda I \end{bmatrix} \mathbf{F} - \begin{bmatrix} \mathbf{G} \\ 0 \end{bmatrix} \right\| \tag{19}$$

if the values of $\|t_{k+1}\|$ or $|\alpha_{k+1}\tau_{k+1}|$ are sufficiently small.

7. Computational results

Three types of calculations were performed. In the first, simulated barcode data along with assumed beam spread functions were used in a forward calculation of the convolution integral in order to determine the characteristics of the blurred images that would be generated. In the second type of calculation, the measured barcode data along with assumed beam spread functions were used in order to estimate ground truth by the LSQR algorithm. Finally, in a third type of calculation, the least squares convolution problem was rewritten in such a fashion that the a beam function could be estimated based on knowledge of the ground truth data and the measured barcode data.

In all of these calculations, several classes of beam spread functions were used in the numerical experiments. These included, for the 10-m data, a constant value over a rectangular area, called an averaging filter. For the 20- and 40-m data, beam spread functions composed of three separate bars of constant values with zero assumed in between the bars were used. These latter spread functions were developed in order to simulate the splitting of the beam into three separate beams beyond 10 m. All of the calculations, of course, had to be done for each of the three widths of the barcodes. Measurements of spot data, used to simulate spike functions, were also used to construct beam spread functions (see Section 7.2 for more details on these functions).

7.1. Developing simulated barcodes for ground truth

Determining ground truth for LADAR scans is not a well-defined process, which makes it difficult to know

whether a reconstruction is acceptable. For example, several issues arise in comparing results to a photograph of the board on which the barcodes were mounted. How far away from the camera should the board be placed in order to construct the proper bar widths and heights? How can we minimize blurring caused by the camera flash against the reflective material? How is a submatrix of greyscale pixels extracted with reasonable ease from the dense digital image generated in a format such as JPEG?

Because of the complexity involved with determining ground truth, it was decided to build simulated ground truth barcode data sets. A base data set of 100×100 intervals was selected, with each interval simulating 10 mm. This would simulate a ground truth board of 1×1 m, the approximate original size of the experimental barcode board shown in Fig. 1. Three data sets were created, representing 25.4 mm (1 in.) bars, 50.8 mm (2 in.) bars and 101.6 mm (4 in.) bars. All of the bars were taken to be 152.4 mm (6 in.) high. The top row bars were separated by 101.6 mm (4 in.), the second row bars were separated by 50.8 mm (2 in.), and the lower three bars were separated by 25.4 mm (1 in.). The intensities were selected to be 230 plus random noise for the bars and 156 plus random noise for the background board. These were chosen based on approximating the values obtained by the LADAR scans. An example of the 25.4 mm (1 in.) simulated data is shown in Fig. 12.

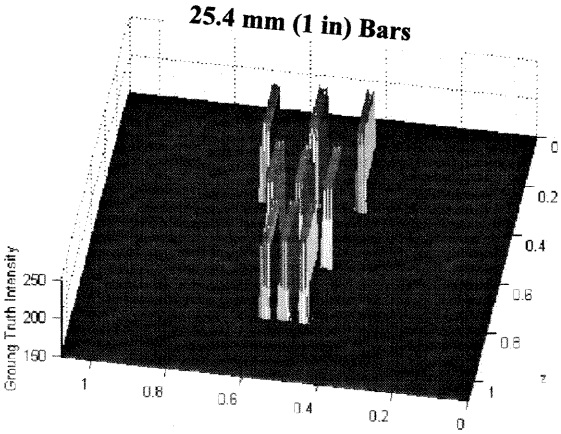

Fig. 12. Simulated ground truth 25.4 mm (1 in.) barcodes.

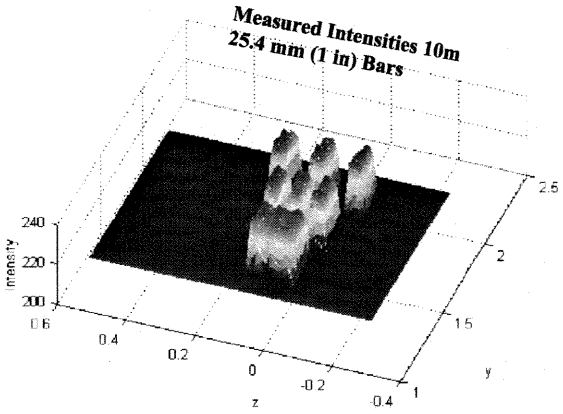

Fig. 13. Measured intensity data for 25.4 mm (1 in.) bars.

7.2. Challenges in estimating a beam spread function

Fig. 13 shows a plot of the scanned data at 10 m. It clearly shows a broadening of the bars as well as a blurring together of the lower three bars. The challenge here is to create a beam spread function that spreads the bars horizontally but not vertically and blends the lower bars together. This blending of the lower bar data may be due to a combined effect of the broadening of neighboring bars and some form of averaging due to the laser beam size. The exact nature of the physical processes involved with the LADAR processing of the data is not in general available due to proprietary concerns of the LADAR manufacturer. Therefore, guesses had to be made on the design of the beam spread function.

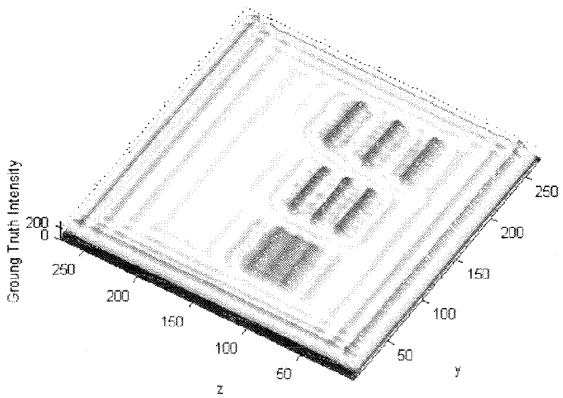

Fig. 14. Reconstructed 25.4 mm (1 in.) bars at 10 m.

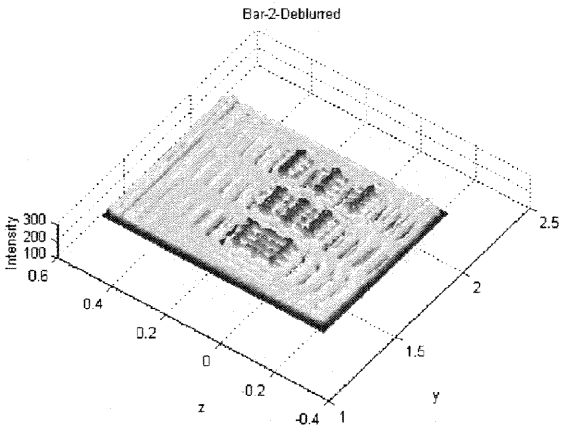

Fig. 15. Partially reconstructed 50.8 mm (2 in.) bars at 10 m.

Based upon the measurements of the LADAR beam described in Section 3, three models of the beam were constructed with one each for 10, 20 and 40 m. For 10 m, a single averaging filter was created and for 20 and 40 m two beam models constructed of three vertical averaging filters each were constructed. All of the beam models were defined in terms of discrete points with grid spacing the same as the grid spacing of the ground truth data sets. The beam models were constructed so that the area under the beam models was unity. Fig. 14 shows the result of reconstructing the 25.4 mm (1 in.) barcode image at 10 m with an averaging filter using LSQR. Fig. 15 shows the partial deconvolution of the 50.8 mm (2 in.) barcode image using the same filter.

The multi-beam spread models were not successful in deconvolving the 20- and 40-m images due likely to the extreme distortion of the reflected LADAR beam caused potentially by beam interference or cross-talk, although this would have to be verified through some form of calibration procedure.

Another class of beam spread function models was constructed. In classic optics, a point spread function for a camera is usually developed by focusing the camera at a small "point" of light in order to simulate as close as possible the effect of a light spike on the camera. This is possible since the camera is a passive instrument in the sense that it gathers light onto its backplane. The LADAR, however, is active in the sense that it produces a beam that is scattered off of a

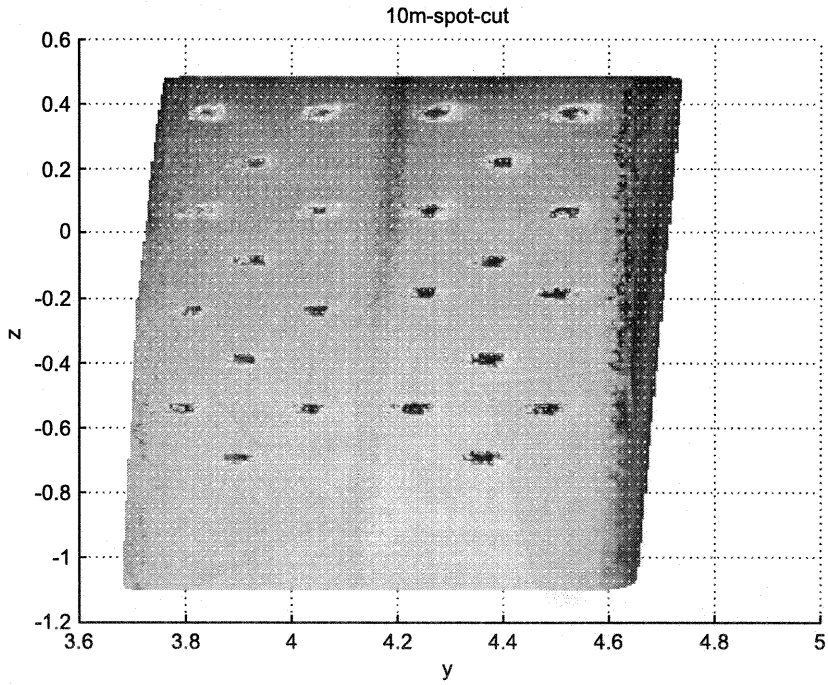

Fig. 16. LADAR images at 10 m of 6.35 mm (1/4 in.) spots in the left three columns and 12.7 mm (1/2 in.) spots in the right columns.

target and then gathers the reflected light into its optical processing unit. Therefore, in order to simulate a spike of light, small dots of the reflective material were placed on a black background and scanned by the LADAR. Fig. 16 shows the reflected image of two sizes of spots. On the left are 6.35 mm (1/4 in.) diameter spots and on the right are 12.7 mm (1/2 in.) diameter spots.

It is clear from the spot images that there is a significant horizontal spread compared to the vertical spread. The distribution of the background color was due to the fact that the background board leaned slightly with the bottom of the board closer to the LADAR. The resulting beam spread functions reflected the larger horizontal to vertical ratio. Fig. 17 shows the result of a deconvolution calculation using a beam spread function with an 11/3 data ratio of horizontal to vertical.

The result shows a partial deconvolution. Note that the edges of the bars are emphasized rather than the middle of the bars. This may be due to the Gibbs phenomenon that occurs at a sharp edge of data when a least squares fitting algorithm is used to reconstruct the image.

One other approach to reconstructing the barcodes was attempted. The algorithm used was rewritten in such a way that the matrix representing the filter became the ground truth image and the unknown vector was the beam spread function. This was an attempt at reverse engineering the beam spread function. This process had an immediate limitation in that the only ground truth data was the simulated barcode data. A beam spread function was computed by the previous least squares algorithm and, when it was applied directly to the simulated barcode data at 10 m, it produced a distorted image very nearly the same as the measured data. The distorted image obtained by reverse engineering is shown in Fig. 18. However, when the computed beam spread function was used as a filter in the deconvolution

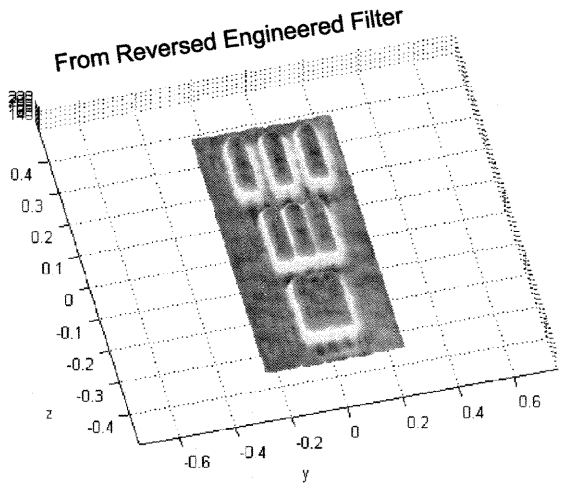

Fig. 18. Distorted 25.4 mm (1 in.) bars based on a least squares estimate of the beam spread function.

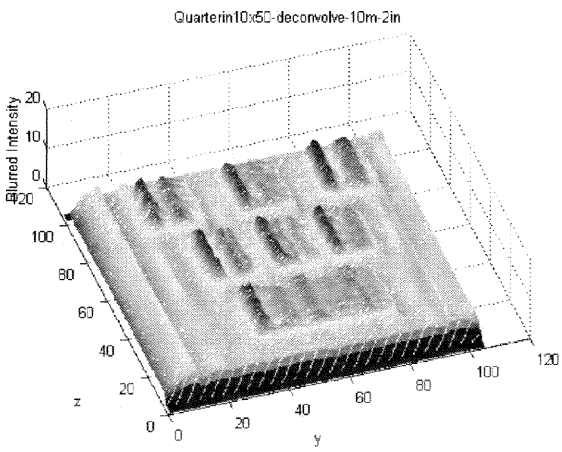

Fig. 17. Deconvolution of 50.8 m (2 in.) barcodes at 10 m using a spot beam spread function.

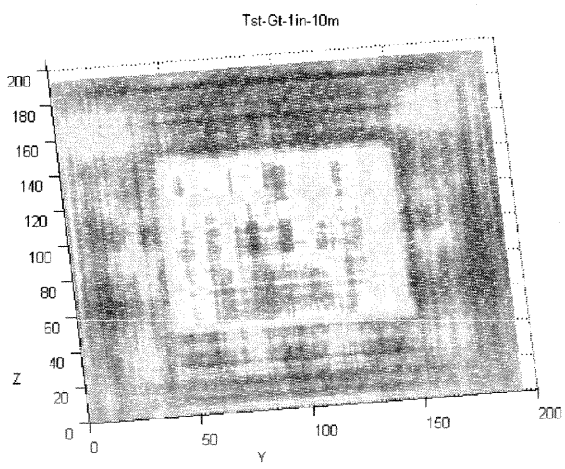

Fig. 19. Reconstructed ground truth image based on the beam spread function from reverse engineering.

procedure, it produced a distorted ground truth image as shown in Fig. 19. This again points out that this problem is very ill conditioned.

8. Discussion and conclusions

In order to determine the effect of beam spread models on ground truth images, one has to determine the nature of ground truth. This is not an easy task and a simple model was used in this study to create the ground truth. The LADAR returns intensity levels in the range 0–255. From measured images, it was determined that the intensity of the return signal of the board on which the bars were mounted was approximately 150 and the intensity levels of the bars were approximately 250. Simulated ground truth data files were created for three sets of barcodes (see ISARC 2001 [1]) with an example of 25.4 mm (1 in.) bars shown in Fig. 12.

Based upon the measurements of the beam spread function, three beam matrices were created to represent the spread function at 10, 20 and 40 m. Since it was difficult to obtain a precise measurement of the beam spread function, matrices representing the three spatial beam spread configurations were created. They were defined in such a manner that the area representing the dark regions was set to zero and the constant value assigned to the light areas was chosen so that the volume under the bright bars summed to unity. With the simulated barcodes and the simulated beam spread functions given, convolution calculations were performed in order to determine how close the simulated distorted images compared to the measured images. The simulated distorted images did not reproduce the horizontal spread distortion observed in the measured images. Although both the ground truth and beam spread images were simulated, it is likely that the lack of prediction was caused mainly by poorly understood beam spread functions. Since the preliminary measurements of the beam spread functions using an infrared scope were crude, this is not surprising. Further study of the physical processes involved with LADAR beams is needed.

As expected, the beam spread function changes at different distances. What was surprising, though, was that a beam spread function could only partially reconstruct different barcodes at the same distance. Thus, the beam spread function computed at 10 m for a given barcode size could not be used to deconvolve the image of the same barcode size obtained at 20 m, but also could not be used to fully reconstruct 50.8 mm (2 in.) barcodes at 10 m. The simulated beam spread function for 10 m was used to recover the ground truth image, and the result is shown in Fig. 14. An attempt was then made to reconstruct the ground truth image for the 50.8 mm (2 in.) bars at 10 m with the same simulated beam spread function. Fig. 15 shows that the full reconstruction was not completely obtained. This suggests that the beam spread function might be influenced by the individual image being deconvolved, especially in the presence of noise. It, therefore, is clear that the nature of the beam spread function and its relation to the image being deconvolved is significant.

An attempt was then made to construct the beam spread function using the least squares algorithm by setting the matrix $\mathbf{H}$ to be the ground truth image and the unknown $\mathbf{F}$ to be the unknown beam spread matrix. Fig. 18 shows the distorted image created for 25.4 mm (1 in.) bars using the best fit Beam Spread matrix. It is very close to the actual data measured for the same bars as given in Fig. 13. However, when used for reconstruction, it clearly fails, as shown in Fig. 19. All of the results, though, point to the fact that reconstructing ground truth from distorted LADAR images is critically dependent on knowledge of the beam spread function and how it relates to individual images.

The partial success obtained from the reconstruction of some barcodes at a distance of 10 m indicates that object identification from LADAR scans is potentially viable. However, to be successful, the object identification procedures appear to require some fundamental physical knowledge that is lacking, such as the nature of LADAR beams, the divergence of the beam, and the scattering characteristics of the scanned target. The internal processing of the returned signal is another unknown since the information may not be available for proprietary reasons. Coarse beam resolution also makes distinguishing fine image elements difficult, if not impossible. This implies that the barcode size and spacing play crucial roles in image reconstruction.

References

[1] W.C. Stone, G.S. Cheok, K.M. Furlani, D.E. Gilsinn, Object identification using bar codes based on LADAR intensity, Proc. of the 18th IAARC/CIB/IEEE/IFAC International Symposium on Automation and Robotics in Construction, ISARC 2001, 10–12 September, Krakow, Poland.

[2] C.C. Paige, M.A. Saunders, Algorithm 583: LSQR: sparse linear equations and least squares problems, ACM Trans. Math. Softw. 8 (2) (1982 Jun) 195–209.

[3] G. Golub, W. Kahan, Calculating the singular values and pseudo-inverse of a matrix, J. SIAM Numer. Anal., Ser. B 2 (2) (1965) 205–224.